Mineralogy and Petrology (2006) 88: 499–526
DOI 10.1007/s00710-006-0124-x

Mineralogy and Petrology
Printed in Austria

Carbonate alteration associated with talc-chlorite mineralization in the eastern Pyrenees, with emphasis on the St. Barthelemy Massif

P. Boulvais[1], **P. de Parseval**[2], **A. D'Hulst**[1,3], and **P. Paris**[4]

[1] Géosciences Rennes – UMR 6118, Université de Rennes I, Campus de Beaulieu, 35042 Rennes cedex, France
[2] Observatoire Midi-Pyrénées – LMTG – UMR5563, 14 avenue Edouard Belin, 31400 Toulouse, France
[3] Département de géologie et de génie géologique, Faculté des sciences et de génie, Université Laval, Sainte-Foy, Québec, Canada G1K 7P4
[4] Talc de Luzenac France, BP 11, 09250 Luzenac cedex, France

Received May 4, 2005; revised version accepted March 7, 2006
Published online April 27, 2006;
Editorial handling: P. Garofalo

Summary

The eastern Pyrenees host a large number of talc-chlorite mineralizations of Albian age (112–97 Ma), the largest of which occur in the St. Barthelemy massif. There talc develops by hydrothermal replacement of dolostones, which were formed by alteration of calcite marbles. This alteration is progressive. Unaltered calcite marbles have oxygen isotope composition of about 25‰ (V-SMOW). The $\delta^{18}O$ values decrease down to values of 12‰ towards the contact with dolostones. This ^{18}O depletion is accompanied by Mg enrichment, LREE fractionation and systematic shifts in the Sr isotope compositions, which vary from $^{87}Sr/^{86}Sr = 0.7087$–0.7092 in unaltered calcite marbles to slightly more radiogenic compositions with $^{87}Sr/^{86}Sr = 0.7094$ near dolomitization fronts. Dolostones have $\delta^{18}O$ values (about 9‰) lower than calcitic marbles, higher REE content and more radiogenic Sr isotope composition ($^{87}Sr/^{86}Sr = 0.7109$ to 0.7130). Hydrothermal calcites have $\delta^{18}O$ values close to dolostones but substantially lower $\delta^{13}C$ values, down to -6.5‰, which is indicative of the contribution of organic matter. The REE content of hydrothermal calcite is one order of magnitude higher than that of calcitic marbles. Its highly radiogenic Sr composition with $^{87}Sr/^{86}Sr = 0.7091$ to 0.7132 suggests that these elements were derived from silicate rocks, which experienced intense chlorite alteration during mineralization. The chemical and isotopic

compositions of the calcite marbles, the dolostones and the hydrothermal calcites are interpreted as products of successive stages of fluid-rock interaction with increasing fluid-rock ratios. The hydrothermal quartz, calcite, talc and chlorite are in global mutual isotopic equilibrium. This allows the calculation of the O isotope composition of the infiltrating water at 300 °C, which is in the $\delta^{18}O_{H_2O} = 2$–4.5‰ range. Hydrogen isotope compositions of talc and chlorite indicate a $\delta D_{H_2O} = 0$ to −20‰. This water probably derived from seawater, with minor contribution of evolved continental water.

Introduction

Talc may form at greenschist facies metamorphic conditions by alteration of ultramafic rocks (*Abzalov*, 1998; *El-Sharkawy*, 2000; *Franceschelli* et al., 2002; *Tesalina* et al., 2003) or dolostones (*Blount* et *Vassiliou*, 1980; *Brady* et al., 1998; *Schandl* et al., 1999; *Hecht* et al., 1999; *Tornos* and *Spiro*, 2000; *Shin* and *Lee*, 2002). Most of the important economic talc deposits are associated with hydrothermal alteration of carbonates (*Moine* et al., 1989), and many of them occur in zones of intense deformation, where enhanced permeability favoured fluid circulation. Formation of metasomatic talc goes in tandem with major chemical changes in the protolith, including addition of silica and H_2O, and removal of calcium and CO_2. The behaviour of magnesium during mineralization is more equivocal. It may, at least in part, originate from the protolith itself (ultramafic rocks or dolostones).

The Trimouns and La Porteille deposits in the St Barthelemy massif (northern Pyrenees, Fig. 1) are two typical examples of talc formation at the expense of dolostones (*Moine* et al., 1989). There are many other deposits of this type in the eastern Pyrenees (*Fortuné*, 1971). In all these deposits, talc mineralization is associated with chloritization of silicate protoliths such as micaschists, gneisses and pegmatites. The relative abundance of talc and chlorite in the talc mineralizations depends on the proportions of dolostone and silicate rocks in the precursor material. For example, in the Las Embollas deposit (Fig. 1a), where dolostones predominate over schists (carbonate-type deposit), talc is abundant and chlorite is nearly absent. On the contrary, in the Ceret and Col de Jau deposits (Fig. 1a) where no host carbonates can be observed (silicate-type deposit), the ore is chlorite-rich. The St. Barthelemy deposits (Trimouns and La Porteille) show approximately equal quantities of talc and chlorite. This is why they may provide information on the mineralization event in both the silicate and carbonate environments. In this paper, we investigate the conditions of fluid-rock interaction including fluid origin, elements source and fluid to rock ratios. We argue for a marine origin of the mineralising fluids on a Pyrenean scale. Carbonates of the St. Barthelemy massif recorded the progressive overprint of interaction with the mineralising fluids by subtle alteration of calcitic marbles, then dolomitization and ultimately precipitation of hydrothermal calcite.

Geological context

The Pyrenean region was affected by the Hercynian and Alpine orogenies. During the Hercynian orogeny (*ca.* 350–300 Ma), polyphase shortening was followed

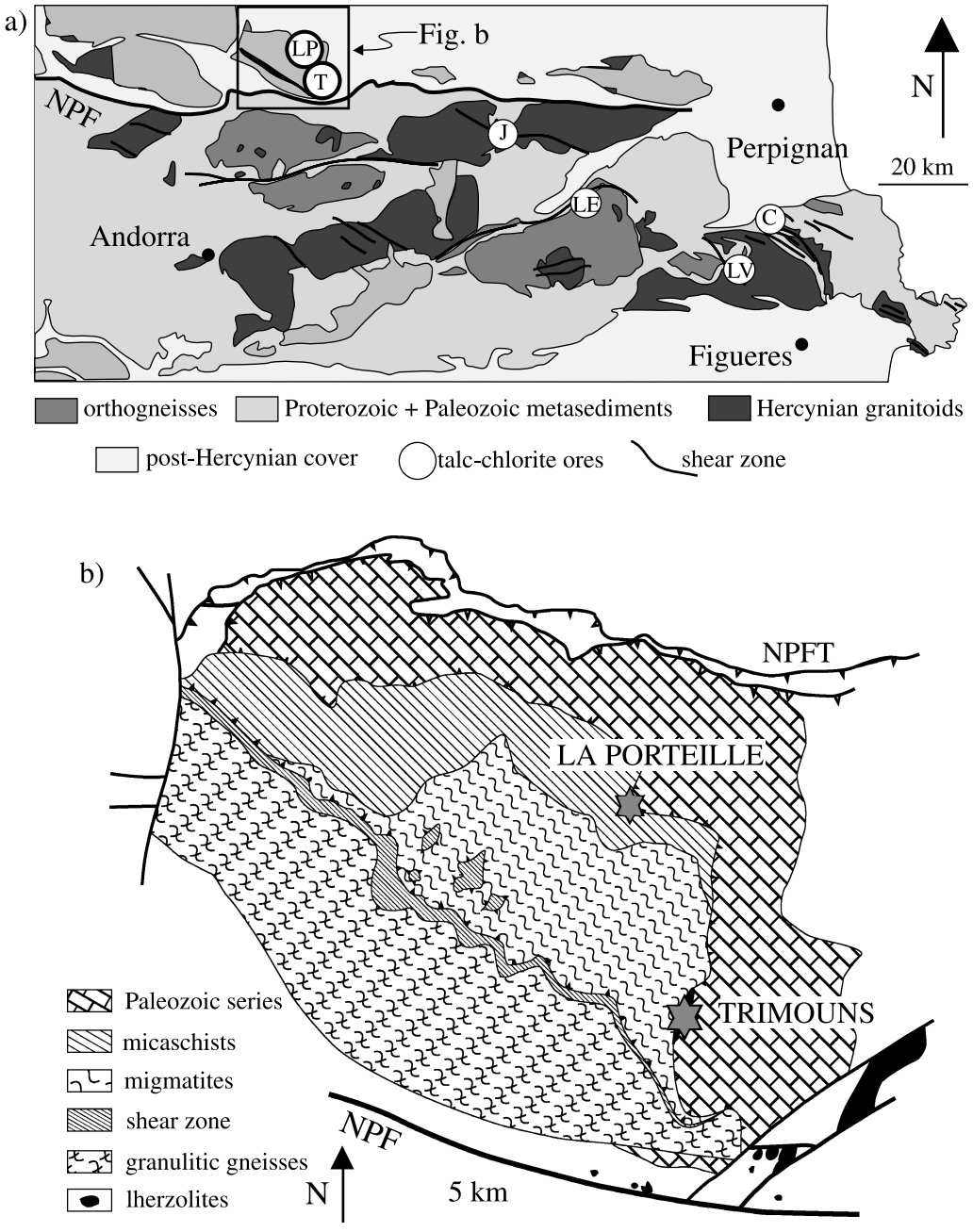

Fig. 1. **a** Simplified geological map of the central and eastern Pyrenees (after *Carreras*, 2001) showing the location of major talc-chlorite deposits (empty circles; LP: La Porteille; T: Trimouns; J: Col de Jau; LE: Las Embollas; LV: La Vajol; C: Ceret). NPF: North Pyrenean Fault. **b** Geological map of the St Barthelemy massif (after *de Saint Blanquat* et al., 1990). NPFT: North Pyrenean Front Thrust

by high temperature – low pressure metamorphism, migmatization and granitic magmatism, which was coeval with dextral transpressional deformation (*Soula* et al., 1986; *Gleizes* et al., 1997, 1998).

During the Alpine orogeny (*ca.* 100–50 Ma), sinistral transtensional movements along the North Pyrenean Fault (NPF) accommodated the eastwards rotation of the Iberian plate and the opening of the Bay of Biscay (Albian period; *Choukroune* et al., 1973; *Choukroune*, 1992; *Olivet*, 1996). At the same time, pull-apart basins developed and were filled with several kilometres of calcareous shales and sandstones (*Puigdefàbregas* and *Souquet*, 1986). During this period, intense hydrothermal activity lead to the formation of talc-chlorite mineralizations in the eastern Pyrenees, especially at the Trimouns and La Porteille regions in the St. Barthelemy massif (Fig. 1). The St. Barthelemy massif may be described as a crustal horst, which is bounded by conjugated normal faults. The exceptional size of the Trimouns deposit (400 000 tons of talc-chlorite ore produced per year) might be related to its position along the NPF and in the St. Barthelemy massif. At the eastern edge of the massif, the NPF bends around the massif (Fig. 1a). This area resembles a pressure-shadow zone of lithospheric scale, which may have focused the flux of mineralizing fluids through steeply dipping faults, finally giving rise to the large Trimouns deposit. Based on U–Pb dating on xenotime and monazite from geode cavities close to the talc ore body at the Trimouns quarry, the duration of hydrothermal activity is estimated to have been 15 Ma (from about 112 to 97 Ma; *Schärer* et al., 1999).

Fluid inclusion data have been obtained from various minerals (quartz, calcite, apatite, allanite) associated with the formation of talc-chlorite at Trimouns (*de Parseval* et al., 1993; *Boiron* et al., 2005). Mineralising fluids were highly saline brines (up to 30 wt% eq. NaCl) and estimated P–T conditions are 250–300 °C at about 2 kbar.

Sampling strategy

The Trimouns and La Porteille quarries display the same structural setting and lithological succession (Fig. 2). Dolostones are more massive and talc-chlorite mineralization is developed more intensely at Trimouns than at La Porteille. The extent of both dolomitization and talc mineralization suggests more prominent fluid circulation in the Trimouns deposit than in the La Porteille deposit. This is why the La Porteille deposit may be regarded as a small-scale analog of the Trimouns deposit.

At Trimouns, sampling was done on a larger scale than at La Porteille. Devonian marbles were sampled hundreds of meters away from the ore zone (Table 1). These samples do not represent the exact protolith of the Ordovician mineralized dolostones. They derive, however, from marine carbonate and the alteration they underwent is likely to provide information on the early stages of the dolomitization event. Some dolostones, which are embedded in the talc ore in the Trimouns quarry (e.g., TRI 00-115), were sampled because they represent the final product of the dolomitization event and the initial product of the talc mineralization one.

At La Porteille, various Ordovician calcitic marbles and dolostones were collected on a smaller scale. We used these chemical analyses because the calcitic protoliths of dolostones are better preserved in this locality and comparison with the REE data from Trimouns is possible (*de Parseval*, 1992).

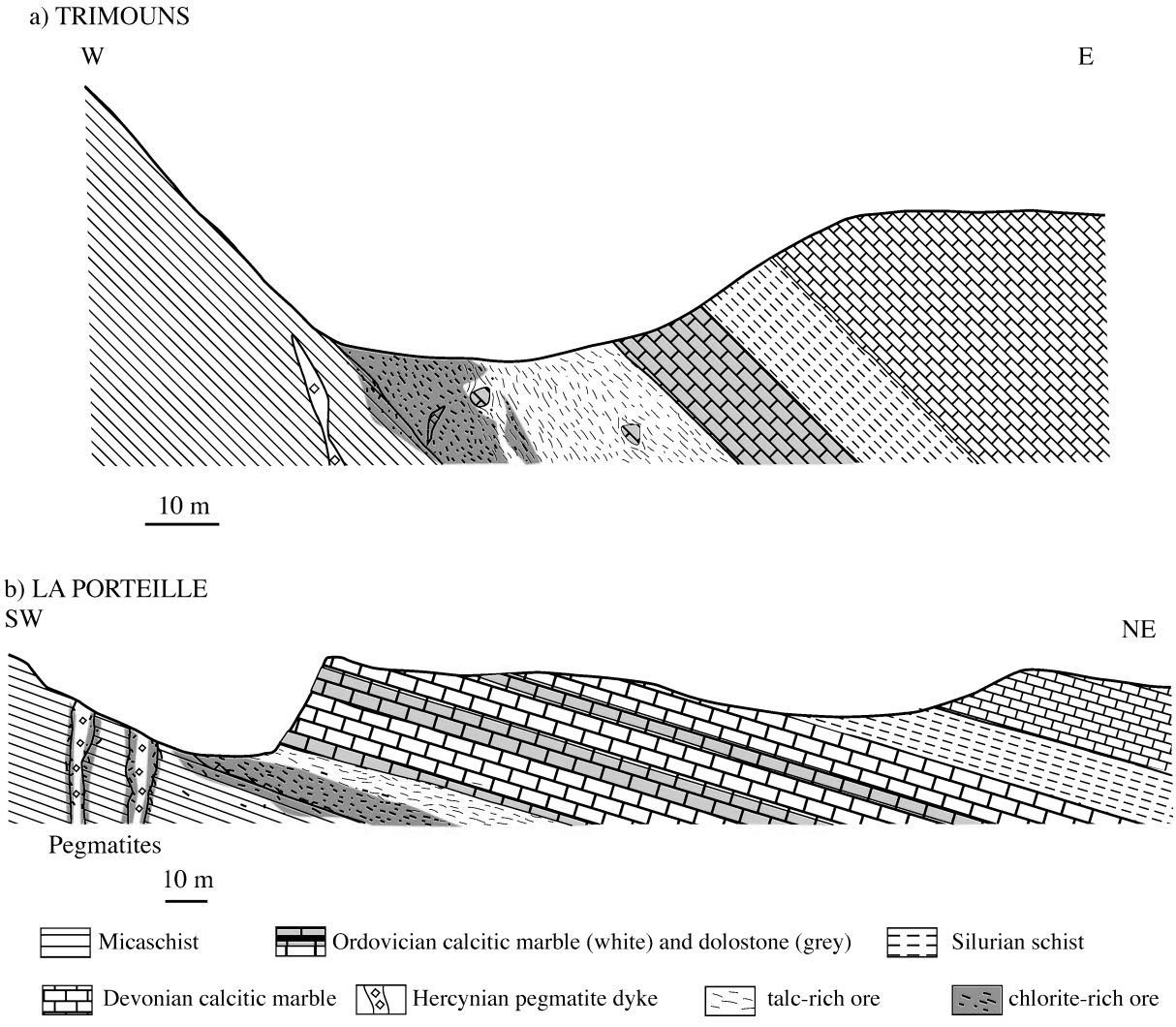

Fig. 2. Schematic cross-sections through Trimouns (**a**) and La Porteille (**b**) talc-chlorite deposits. At Trimouns, Ordovician marbles are completely dolomitized. Residual dolostones and pegmatite nodules are embedded in the talc-chlorite ore. At La Porteille, three dolomitized levels are exposed

In all localities, various samples of talc and chlorite ores were collected, as well as hydrothermal calcite veins (all quarries but Ceret, Fig. 1). Quartz + chlorite veins within chloritized micaschists were also sampled as well as euhedral quartz crystals in empty voids (Col de Jau). These minerals precipitated directly from the mineralising fluids. Their stable isotope compositions (O, C and H) are likely to bring information on fluids source and allow us to compare the different ore bodies on a Pyrenean scale. Sr isotopic compositions of carbonates were determined in order to constrain the origin of elements carried by fluids.

Table 1. *O, H (vs. SMOW), C (vs. PDB) and Sr isotope compositions of samples from a) Trimouns deposit, b) La Porteille deposit and c) other talc-chlorite deposits in the Pyrenees*

Sample	Description	Distance to ore (m)	Cal/Dol	Cal		Dol		Qz	Tlc		Chl		$^{87}Sr/^{86}Sr$	$\pm 2\sigma_m$
				$\delta^{18}O$	$\delta^{13}C$	$\delta^{18}O$	$\delta^{13}C$	$\delta^{18}O$	$\delta^{18}O$	δD	$\delta^{18}O$	δD		
a) Trimouns														
TRI 02-37a	dolomitized marble	600	0.93	11.0	−1.10	9.6	−0.52							
TRI 02-37b	dolomitized marble	600	1.04	11.4	−1.80	10.0	−0.19							
TRI 02-38	dolomitized marble	450	0.73	9.7	−1.42	9.3	−0.02							
TRI 02-39	dolomitized marble	350	0.20	10.8	0.02	9.8	0.39							
TRI 02-40	dolomitized marble	200	0.22	10.0	−0.53	8.9	−0.09							
TRI 02-41	dolomitized marble	150	0.26	10.3	0.23	9.0	0.66							
TRI 02-42	dolostone	100	0			8.8	0.64							
TRI 02-43	dolostone	50	0			10.4	0.01							
T400A	dolostone	0				8.7	−0.39						0.712992	8
T151	dolostone	0				7.8	0.17						0.711536	9
TRI 00-130	dolostone	0				9.0	0.61							
TRI 00-131b	dolostone	0				8.1	0.48							
TRI 00-116	talc-bearing dolostone	0		9.9	0.06	9.1	0.78							
TRI 00-48	talc-bearing dolostone	0				8.7	−0.31							
TRI 00-49	talc-bearing dolostone	0				7.7	−0.28							
TRI 00-127a	talc-bearing dolostone	0				8.0	−0.28							
TRI 00-115a/D1.50	dolomitic nodule (1.5 cm from pressure shadow)					8.5	0.95							
TRI 00-115a/D0.68	dolomitic nodule (0.68 cm from pressure shadow)					8.8	1.12							
TRI 00-115a/D0.23	dolomitic nodule (0.23 cm from pressure shadow)					8.6	1.00							
TRI 00-115a/DT0.81	pressure shadow (0.81 cm from dolomitic nodule)					7.8	0.76							
TRI 00-115a/DT0.16	pressure shadow (0.16 cm from dolomitic nodule)					7.9	0.08							
TRI 00-115a/TD0.14	pressure shadow (0.14 cm from dolomitic nodule)					8.3	0.81							
TRI 00-115b/D0.28	dolomitic nodule (0.28 cm from talc)					8.5	1.16							
TRI 00-115b/D0.0	dolomitic nodule (close to talc)					8.5	1.05							
TRI 00-115b/DT1.64	pressure shadow (1.64 cm from dolomitic nodule)					7.6	0.11							
TRI 00-115b/DT0.21	pressure shadow (0.21 cm from dolomitic nodule)					7.9	0.70							
TRI 00-102	hydrothermal calcite			8.5	−2.89									
TRI 01-221	hydrothermal calcite			8.6	−2.24								0.711373	9

(*continued*)

Table 1 (*continued*)

Sample	Description	Distance to ore (m)	Cal/Dol	Cal		Dol		Qz	Tlc		Chl			
				$\delta^{18}O$	$\delta^{13}C$	$\delta^{18}O$	$\delta^{13}C$	$\delta^{18}O$	$\delta^{18}O$	δD	$\delta^{18}O$	δD	$^{87}Sr/^{86}Sr$	$\pm 2\sigma_m$
TRI 01-222	hydrothermal calcite			8.5	−3.82								0.711275	6
TRI 01-223	hydrothermal calcite			8.3	−0.65								0.710806	8
TRI 01-224	hydrothermal calcite			8.5	−2.70									
TRI 01-225	hydrothermal calcite			8.7	−1.53									
Tlc-SF	white hydrothermal talc								6.3					
TRI 00-115	white hydrothermal talc								6.2	−48.9				
TRI 00-117	white hydrothermal talc								6.3	−44.7				
TRI 00-118	white hydrothermal talc								6.3					
TRI 00-119	white hydrothermal talc								6.2	−41.3				
TRI 00-120	white hydrothermal talc								6.4					
TRI 00-121	white hydrothermal talc								6.3					
TRI 00-122	white hydrothermal talc								6.2					
TRI 00-123	white hydrothermal talc								6.3					
TRI 00-124	white hydrothermal talc								6.1					
TRI 00-126	grey talc								5.7					
TRI 00-127b	talc from talc-bearing dolostone								5.6					
Chl-SF	pale green chlorite (after pegmatite)										4.6			
Tri 4	pale green chlorite (after pegmatite)										5.0			
TRI 00-111	pale green chlorite (after pegmatite)										5.3			
TRI 00-112	pale green chlorite (after pegmatite)										4.6			
TRI 00-113	pale green chlorite (after pegmatite)										4.6			
TRI 00-114	pale green chlorite (after pegmatite)										5.6	−47.2		
T 254	dark green chlorite (after micaschist)										4.7			
TRI 00-109	dark green chlorite (after micaschist)										4.6			
TRI 00-110	dark green chlorite (after micaschist)										4.6	−40.2		
TRI 00-103	quartz-chlorite vein							10.2			4.8			
TRI 00-104	quartz-chlorite vein							11.2			5.8			
TRI 00-105	quartz-chlorite vein							10.1			5.1			

(*continued*)

Table 1 (*continued*)

Sample	Description	Distance to ore (m)	Cal		Dol		Qz	Tlc		Chl			
			$\delta^{18}O$	$\delta^{13}C$	$\delta^{18}O$	$\delta^{13}C$	$\delta^{18}O$	$\delta^{18}O$	δD	$\delta^{18}O$	δD	$^{87}Sr/^{86}Sr$	$\pm 2\sigma_m$
b) La Porteille													
POR 02-1	Ordovician calcitic marble	45	20.1	1.38								0.708741	8
POR 02-2	Ordovician calcitic marble	40	16.1	0.87								0.709143	8
POR 02-3	Ordovician calcitic marble	40	24.5	1.41								0.708857	8
POR 02-4	Ordovician calcitic marble	30	15.4	1.59								0.708678	7
POR 02-6a	calcite vein within calcitic marble	25	10.6	−1.77									
POR 02-6b	partially dolomitized marble	25	11.4	−0.56	10.00	−0.50							
POR 02-7	Ordovician calcitic marble	15	19.1	1.45								0.709244	5
POR 02-8	Ordovician calcitic marble	15	24.5	1.40								0.708971	8
POR 02-10	Ordovician calcitic marble	15	12.8	1.20								0.709365	7
POR 02-10a	id, 3 cm from dolomitization front	20	12.3	0.61									
POR 02-10b	id, 8 cm from dolomitization front	20	12.4	1.12									
POR 02-11	dolostone	5			9.05	−0.52						0.710962	
POR 02-12	hydrothermal calcite		8.6	−2.32								0.710929	8
POR 02-13	hydrothermal calcite		8.5	−4.42								0.711388	7
POR 03-1	hydrothermal calcite		9.9	−2.32								0.713195	8
POR 02-14	white hydrothermal talc							6.2					
POR 02-15	white hydrothermal talc							6.2					
POR 02-18	white hydrothermal talc							6.2					
POR 02-19	white hydrothermal talc							6.2					
POR 02-20	pale green chlorite									4.7			
POR 02-21	pale green chlorite									4.8			
POR 02-22	dark green chlorite									4.5			
POR 02-23	dark green chlorite									4.8			
POR 02-31	dark green chlorite									4.8	−47.6		
POR 02-32	dark green chlorite									4.8			
POR 02-34	quartz veinlet within chloritized micaschists						11.1						
POR 02-35	quartz veinlet within chloritized micaschists						11.2						

(*continued*)

Table 1 (*continued*)

Sample	Location	Description	Cal		Qz	Tlc		Chl			
			$\delta^{18}O$	$\delta^{13}C$	$\delta^{18}O$	$\delta^{18}O$	δD	$\delta^{18}O$	δD	$^{87}Sr/^{86}Sr$	$\pm 2\sigma_m$
c) Other ore deposits											
JAU 00-91	Col de Jau	hydrothermal calcite	7.4	−6.70							
JAU 01-210	Col de Jau	hydrothermal calcite	9.7	−3.94						0.711821	8
JAU 01-211	Col de Jau	hydrothermal calcite	7.6	−6.55							
JAU 01-212	Col de Jau	hydrothermal calcite	8.3	−6.45						0.711317	9
JAU 01-213	Col de Jau	hydrothermal calcite	7.7	−0.42						0.711085	8
JAU 01-219a	Col de Jau	chlorite-bearing talc ore				5.2					
JAU 01-219b	Col de Jau	chlorite-bearing talc ore				5.3					
JAU 01-220a	Col de Jau	chlorite-bearing talc ore				5.5					
JAU 01-220b	Col de Jau	chlorite-bearing talc ore				5.5					
JAU 00-90	Col de Jau	chloritite						4.5	−50.2		
JAU 00-96	Col de Jau	chloritite						4.7			
JAU 01-214	Col de Jau	hydrothermal quartz			9.6						
JAU 01-215	Col de Jau	hydrothermal quartz			10.4						
JAU 01-216	Col de Jau	hydrothermal quartz			10.3						
EMB 01-178a	Las Embollas	calcite vein in host rock	10.8	0.29							
EMB 01-181a	Las Embollas	calcite vein in host rock	9.3	0.14						0.708613	7
EMB 01-174	Las Embollas	hydrothermal calcite	11.6	0.43						0.709132	9
EMB 01-175	Las Embollas	hydrothermal calcite	10.7	−0.26							
EMB 01-176	Las Embollas	hydrothermal calcite	7.8	0.67							
EMB 01-177	Las Embollas	hydrothermal calcite	8.6	−0.54						0.709262	8
EMB 01-170	Las Embollas	hydrothermal white talc				5.8	−49.4				
EMB 01-171	Las Embollas	hydrothermal white talc				5.9					
EMB 01-172	Las Embollas	hydrothermal white talc				6.4					
REY 01-190	Ceret	quartz vein			9.7						
REY 01-191	Ceret	quartz vein			7.0						
REY 01-192	Ceret	quartz vein			7.3						
REY 01-186	Ceret	chloritite						2.8			
REY 01-187	Ceret	chloritite						3.0	−60.5		
REY 01-188	Ceret	chloritite						2.9			

(*continued*)

Table 1 (*continued*)

Sample	Location	Description	Cal		Qz	Tlc		Chl			
			$\delta^{18}O$	$\delta^{13}C$	$\delta^{18}O$	$\delta^{18}O$	δD	$\delta^{18}O$	δD	$^{87}Sr/^{86}Sr$	$\pm 2\sigma_m$
REY 01-189	Ceret	chloritite						2.7			
REY 01-183	Ceret	chloritite						3.1			
VAJ 01-206	La Vajol	hydrothermal calcite	8.4	−2.34							
VAJ 01-207	La Vajol	hydrothermal calcite	8.4	−1.90						0.712484	8
VAJ 01-208	La Vajol	hydrothermal calcite	8.5	−2.43						0.712821	8
VAJ 01-209	La Vajol	hydrothermal calcite	8.1	−2.32							
VAJ 01-200	La Vajol	chlorite-bearing talc ore				5.4					
VAJ 01-201	La Vajol	chlorite-bearing talc ore				5.3	−42.2				
VAJ 01-202	La Vajol	chlorite-bearing talc ore				5.7					
VAJ 01-203	La Vajol	chlorite-bearing talc ore				5.7					
VAJ 01-196	La Vajol	chloritite						4.1			
VAJ 01-198	La Vajol	chloritite						4.1			
VAJ 01-199	La Vajol	chloritite						4.0			
VAJ 01-194	La Vajol	chloritite						4.4			
VAJ 01-195b	La Vajol	chloritite						3.9			

Table 2. *Chemical composition of calcitic marbles, dolostone and hydrothermal calcite from the La Porteille quarry. Major elements are given in oxide weight percent, trace elements in ppm. dl: detection limit*

Sample	POR 02-1	POR 02-2	POR 02-3	POR 02-4	POR 02-7	POR 02-8	POR 02-10	POR 02-11	POR 02-12	POR 03-1
Type	Marble	Marble	Marble	Marble	Marble	Marble	Marble	Dolostone	Calcite	Calcite
wt%										
SiO_2	<dl	1.21	0.49	1.29	<dl	0.23	<dl	<dl	<dl	0.27
Al_2O_3	<dl	0.37	0.18	0.36	<dl	0.13	0.2	<dl	<dl	<dl
Fe_2O_3	<dl	<dl	<dl	<dl	<dl	<dl	<dl	0.49	<dl	<dl
MnO	<dl	0.04	<dl	0.03	<dl	<dl	0.03	0.03	<dl	0.04
MgO	<dl	0.58	0.21	0.79	0.15	0.16	0.24	19.54	0.33	0.23
CaO	55.1	54.4	55.6	53.6	55.9	55.7	55.8	32.9	56.0	55.1
Na_2O	<dl	<dl	<dl	<dl	<dl	<dl	<dl	<dl	<dl	<dl
K_2O	<dl	<dl	<dl	<dl	<dl	<dl	<dl	<dl	<dl	<dl
TiO_2	<dl	<dl	<dl	<dl	<dl	<dl	<dl	<dl	<dl	<dl
P_2O_5	<dl	<dl	<dl	<dl	<dl	<dl	<dl	<dl	<dl	<dl
LOI	43.2	42.3	42.1	42.4	43.1	43.1	43.0	46.6	43.1	43.1
Total	98.36	98.81	98.59	98.50	99.11	99.33	99.33	99.52	99.46	98.75
ppm										
La	1.04	0.72	1.13	1.44	2.81	2.81	1.02	14.0	33.0	22.6
Ce	1.49	1.68	1.95	2.72	3.90	3.60	1.71	27.2	104	56
Pr	0.22	0.29	0.25	0.35	0.53	0.55	0.26	3.28	16.0	8.2
Nd	0.97	1.49	1.02	1.36	2.18	2.28	1.22	11.2	72.4	36.4
Sm	0.26	0.51	0.21	0.31	0.45	0.49	0.37	1.54	19.4	9.99
Eu	0.08	0.13	0.07	0.06	0.10	0.11	0.09	1.77	1.68	2.01
Gd	0.31	0.60	0.21	0.30	0.55	0.51	0.49	1.18	19.7	11.1
Tb	0.04	0.09	0.03	0.05	0.09	0.08	0.08	0.15	3.35	2.01
Dy	0.25	0.49	0.19	0.29	0.56	0.50	0.48	0.81	20.4	13.0
Y	2.35	3.48	1.66	2.08	5.78	5.39	5.18	6.26	153	105
Ho	0.05	0.09	0.04	0.06	0.12	0.11	0.10	0.15	4.08	2.73

(*continued*)

Table 2 (*continued*)

Sample	POR 02-1	POR 02-2	POR 02-3	POR 02-4	POR 02-7	POR 02-8	POR 02-10	POR 02-11	POR 02-12	POR 03-1
Type	Marble	Marble	Marble	Marble	Marble	Marble	Marble	Dolostone	Calcite	Calcite
Er	0.14	0.21	0.11	0.15	0.33	0.29	0.28	0.41	11.7	7.94
Tm	0.02	0.03	0.02	0.02	0.04	0.04	0.04	0.06	1.77	1.19
Yb	0.10	0.15	0.09	0.12	0.25	0.23	0.21	0.37	12.1	7.89
Lu	0.02	0.02	0.01	0.02	0.04	0.03	0.03	0.05	1.80	1.13
Ba	11.2	5.38	15.7	<dl	8.97	18.9	6.56	<dl	<dl	<dl
Sr	146	110	172	182	192	195	123	40.5	111	160
Rb	<dl	<dl	0.93	<dl	1.10	0.85	<dl	<dl	<dl	<dl
Cs	<dl	<dl	<dl	<dl	<dl	<dl	<dl	<dl	<dl	<dl
U	0.08	0.10	0.06	0.16	0.32	0.58	1.39	0.18	<dl	0.03
Th	0.12	0.28	0.29	0.34	0.34	0.37	0.22	0.05	0.01	0.02
Pb	5.81	9.18	1.90	10.8	2.25	4.59	<dl	<dl	<dl	<dl
Ta	0.01	0.04	0.02	0.04	0.02	0.02	0.02	<dl	0.01	0.01
Nb	0.15	0.40	0.29	0.50	0.21	0.19	0.17	<dl	<dl	<dl
Zr	2.34	4.34	2.88	7.00	2.70	3.19	2.43	<dl	<dl	<dl
Hf	0.06	0.12	0.08	0.19	0.08	0.08	0.06	<dl	0.05	0.04
Ni	5.93	6.15	6.07	6.20	6.77	6.92	5.64	<dl	4.92	4.44
Cr	<dl	<dl	<dl	<dl	<dl	<dl	<dl	<dl	<dl	<dl
Co	0.80	0.74	0.75	1.03	0.83	0.69	0.67	0.34	0.51	0.54
Cu	<dl	<dl	<dl	<dl	<dl	<dl	<dl	<dl	<dl	<dl
V	<dl	2.48	2.07	2.68	1.93	2.20	<dl	1.77	<dl	<dl
Mo	<dl	<dl	<dl	<dl	<dl	<dl	<dl	<dl	<dl	<dl
Sn	<dl	<dl	<dl	<dl	<dl	<dl	<dl	<dl	<dl	<dl
W	<dl	0.32	<dl	0.29	0.82	<dl	<dl	<dl	<dl	<dl
Zn	<dl	<dl	<dl	9.67	9.89	<dl	<dl	<dl	<dl	<dl

Analytical methods

Samples were finely ground in an agate mortar before acid dissolution (HNO_3). Chemical compositions (Table 2) have been obtained by ICP-AES (major elements) and ICP-MS (trace elements) at the SARM laboratory (CRPG-CNRS, Nancy, France). Analytical uncertainties were from ±2‰ (CaO) to ±15% for major and trace elements depending on concentration level. Detection limits were from 0.03% (MnO) to 0.2% (SiO_2) for major elements; and from 0.005 ppm (Lu, Yb) to 8 ppm (Zn) for trace elements.

Oxygen and carbon isotope compositions (Table 1) were measured on a VG SIRA 10 triple collector mass spectrometer at the geochemical laboratory of Géosciences, University of Rennes 1. CO_2 was liberated from calcite and dolomite by reaction with anhydrous H_3PO_4 at 25 and 50 °C for 12 hours (*McCrea*, 1950). We employed a selective extraction technique to separate the CO_2 which is derived from calcite and dolomite (e.g., *Al-Aasm* et al., 1990). CO_2 liberated after 2 hours of reaction at 25 °C is considered to come from calcite. Vessels were then evacuated before a second step of overnight acid digestion at 50 °C. The amount of CO_2 released during each step was measured on a Hg manometer in order to estimate the relative proportions of calcite and dolomite. Replicate analyses of reference material NBS 29 yielded $\delta^{18}O = 28.68 \pm 0.10$‰ and $\delta^{13}C = 1.91 \pm 0.04$‰, which is in good agreement with recommended values of 28.65‰ and 1.95‰, respectively. Internal standards were used to calibrate the procedure. The O isotope composition of silicates was measured after overnight reaction with BrF_5 at 670 °C (*Clayton* and *Mayeda*, 1963) and conversion into CO_2 by reaction with hot graphite. Results were corrected by adding 0.3‰ to measured values considering long term analysis of internal standards and NBS 28 ($\delta^{18}O = 9.3 \pm 0.1$‰). Analytical precision including standard correction and internal reproducibility is estimated at ±0.2‰ for O in silicates and about 0.15‰ for O and better than 0.1‰ for C in carbonates.

The H isotope composition was measured on molecular H_2 after reduction of H_2O with hot U (*Bigeleisen* et al., 1952) on a δE Finnigan Mat instrument at the geochemical laboratory of IPGP, University of Paris VII. The reproducibility of analyses is ±2‰.

Sr isotope analyses were performed on carbonate samples at the geochemical laboratory of Géosciences, University of Rennes 1, using a Finnigan Mat 252 mass spectrometer. About 40 mg of each sample were dissolved in 2*N* cold HCl for one hour. Solutions were then dried and redissolved in HNO_3 for Sr-Spec single-step column chemical separation. Total Sr blank was better than 50 pg and is considered as being negligible. All $^{87}Sr/^{86}Sr$ ratios were corrected for mass fractionation relative to $^{86}Sr/^{88}Sr = 0.1194$. During the course of analyses, NBS 987 gave a mean Sr isotope ratio of $^{87}Sr/^{86}Sr$ of 0.710261 ± 5 (1, $\sigma n = 10$). The isotopic ratios were not adjusted to any standard values.

Petrography

In the St. Barthelemy massif, calcitic marbles have a penetrative foliation parallel to the stratification. Kinematic indicators such as asymmetric fibres in pressure

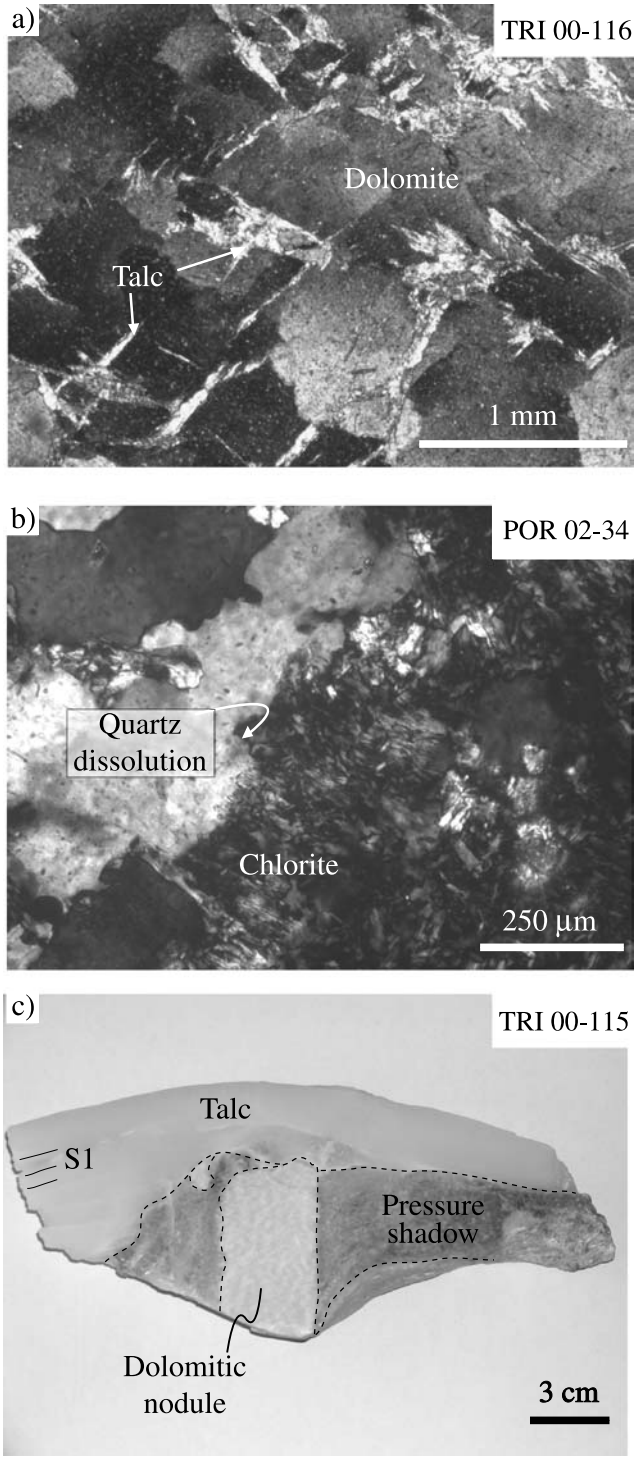

Fig. 3. **a** Talc-bearing dolostone of Trimouns. Talc develops at grain contacts and within dolomite twins (crossed polarizers). **b** Partially chloritized micaschist with residual quartz from La Porteille. Quartz grains are dissolved and replaced by chlorite (crossed polarizers). **c** Hand-specimen of a dolostone nodule surrounded by white hydrothermal foliated talc and pressure shadows. Nodule and pressure shadows are delineated by dotted lines. S1 = foliation

fringes around quartz nodules indicate top-to-the-South-West thrusting. Because of the later tilting to the North, this apparent thrusting movement may correspond to normal shearing at the time of deformation.

Dolostones are mostly undeformed (Fig. 3a). At Trimouns, a progressive increase in dolomite fraction of calcitic marbles towards the ore is documented over a few hundred meters (Table 1). At La Porteille, three levels of dolostones are visible (Fig. 2b). They are separated from calcitic marbles by sharp dolomitization fronts. Some calcite veins are located within the dolostone levels. Incipient talc crystallisation at dolostone grain contacts is believed to have occurred as strain free conditions, because talc crystals are not oriented (Fig. 3a). The same is true for chlorite growth in silicate rocks (Fig. 3b). In marked contrast with dolostones, the talc-chlorite ore bodies are highly foliated in all Pyrenean quarries. Some nodules are wrapped by the talc foliation and talc grew on the expense of dolomite in pressure shadows (Fig. 3c). In talc ore, the conservation of structures such as sedimentary bedding, which was initially present in the carbonate precursors, led *Moine* et al. (1989) to propose the following near constant volume transformation:

$$2CaMg(CO_3)_2 + Mg^{2+} + 4SiO_{2(aq)} + 2H^+ = Mg_3Si_4O_{10}(OH)_2 + 2Ca^{2+} + 4CO_2$$

Hydrothermal calcite veins are abundant in carbonate-type deposits and cross-cut talc deposits without any clear orientation. Calcite veins are made of large (up to 5 cm at Trimouns) and euhedral calcite crystals.

Results

Carbonates in the St. Barthelemy massif

Chemical analyses on La Porteille samples are reported in Table 2. Calcitic marbles contain small amounts of silicate materials, which results in maximum SiO_2 contents of 1.3 wt% for sample POR 02-4. Dolostones and hydrothermal calcites are essentially free of silicates impurities (e.g., POR 03-1, POR 02-11; Table 2).

The REE + Y compositions of calcitic marbles, dolostones and hydrothermal calcites (Fig. 4) are normalised to Post Archean Australian Shale. Calcitic marbles have low REE contents and depleted and fractionated LREE patterns with a negative Ce anomaly (Fig. 4a), akin to those of marine Paleozoic carbonates from Australia (*Nothdurft* et al., 2004). In contrast, the dolostones and hydrothermal calcites have higher REE concentrations and do not display any significant negative Ce anomaly (Fig. 4b). Dolostone POR 02-11 shows a positive Eu anomaly, whereas hydrothermal calcite POR 02-12 has a negative Eu anomaly.

All carbonates from the St. Barthelemy Massif talc-chlorite deposits exhibit a continuous covariation of their carbon and oxygen isotope ratios (Fig. 5a). The stable isotope compositions of calcite marbles from La Porteille are shifted from unaltered isotopic compositions with close to primary marine values of $\delta^{18}O = 25‰$ and $\delta^{13}C = 1‰$ down to strongly altered compositions with values of $\delta^{18}O = 12‰$ and $\delta^{13}C = -0.5‰$. With values of $\delta^{18}O = 7$ to 10‰ and $\delta^{13}C = +1$ to $-0.5‰$, the stable isotope compositions of the dolostones are a continuation of this depletion trend (Fig. 5a). Hydrothermal calcites have O isotope compositions close to those of dolostones but have lower $\delta^{13}C$ (down to $-4.5‰$ in the St. Barthelemy deposits). Hydrothermal calcites from other deposits have similar $\delta^{18}O$ values to St. Barthelemy hydrothermal calcites, but differ from them by more variable $\delta^{13}C$

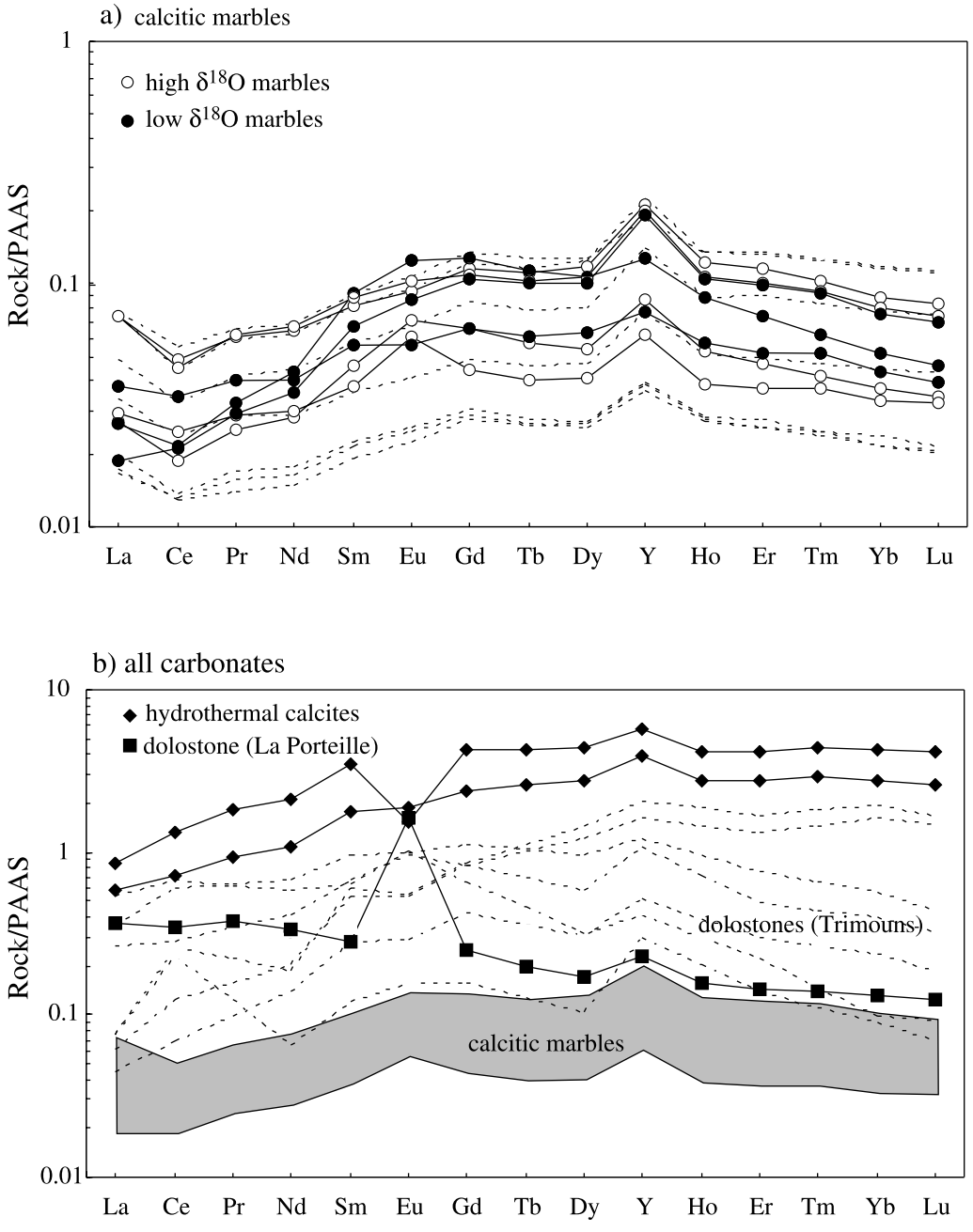

Fig. 4. **a** REE + Y patterns of the La Porteille calcitic marbles (normalisation to Post-Archean Australian Shale; *McLennan*, 1989). Low δ^{18}O marbles (black circles) are POR 02-10, POR 02-4, POR 02-2. Dotted patterns correspond to Australian Devonian marine carbonates (*Nothdurft* et al., 2004). **b** REE + Y patterns of the La Porteille dolostone POR 02-11 (black square) and hydrothermal calcites (black diamonds). Dotted lines correspond to Trimouns dolostones (data from *de Parseval*, 1992). The field of the La Porteille calcitic marbles is the same in both panels

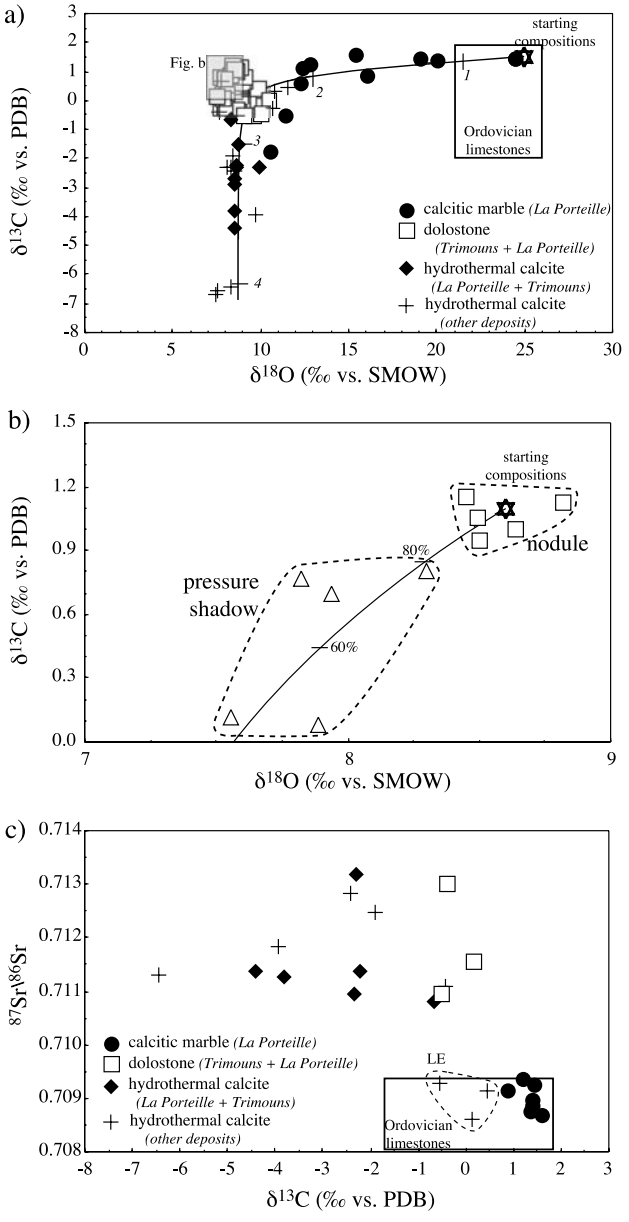

Fig. 5. **a** C and O isotope compositions of carbonates from Trimouns and La Porteille, together with hydrothermal calcite from other talc-chlorite deposits. Reported is also the field of Ordovician marine limestones (*Veizer* et al., 1999) and a model of infiltration at 300 °C using the zero-dimension formula of *Taylor* (1977) for open systems (italic numbers on the curve refer to fluid-rock ratios in atom percent). CO_2 is assumed to be in O isotopic equilibrium with H_2O ($\delta^{18}O_{CO_2}$ calculated with fractionation factors calcite-H_2O and calcite-CO_2 of *Zheng*, 1999). C fractionation factor between calcite and CO_2 is taken from *Bottinga* (1968). **b** Detail of small box in a) showing O and C isotope compositions of dolomite from nodule TRI 00-115 (squares) and from pressure shadow zones (triangles). The theoretical curve of decarbonation is labelled with wt% residual carbonate (see text for explanations). The O isotope fractionation factor between CO_2 and dolomite ($\alpha_{CO_2-Dol} = 1.0076$ at 300 °C) is from *O'Neil* and *Epstein* (1966). C fractionation ($\alpha_{CO_2-Dol} = 1.00129$ at 300 °C) is from *Ohmoto* and *Rye* (1979). **c** Sr isotope composition vs. $\delta^{13}C$ diagram of carbonates from all deposits. The field of Las Embollas (LE) hydrothermal calcites is marked by the dotted line within the Ordovician limestone box

values, which scatter between 0‰ in the carbonate-dominated deposit of Las Embollas and about −6.5‰ in the silicate-dominated deposit of Col de Jau.

In sample TRI 00-115 (Fig. 3c), a rigid dolomitic nodule has $\delta^{18}O$ and $\delta^{13}C$ values of 8.6 ± 0.2‰ and 1.1 ± 0.1‰, respectively, that are higher than those of the dolomite within the pressure shadow zone, which has compositions of $\delta^{18}O = 7.9 \pm 0.4$‰ and $\delta^{13}C = 0.5 \pm 0.4$‰; see also Fig. 5b.

Isotopic compositions of partially dolomitized Trimouns marbles do not show any correlation with distance to the ore (Table 1), despite the fact that the degree of dolomitization increases more or less regularly towards the ore. In these samples, dolomite is enriched in ^{13}C relative to calcite by about 0.5 to 1‰. This is compatible with equilibrium fractionation (e.g., *Ohmoto* and *Rye*, 1979). The dolomite is, however, depleted in ^{18}O relative to calcite (Table 1). This peculiar signature indicates oxygen isotope disequilibrium between calcite and dolomite (*Sheppard* and *Schwarcz*, 1970). It may be hypothesised that calcite was in oxygen isotope equilibrium with the mineralizing fluids during the initial, high temperature stage of dolomitization. This equilibrium state was then perturbed by retrograde isotopic exchange with similar fluids during subsequent lower temperature stages of fluid-rock interaction, which gave rise to an increase of $\delta^{18}O$ values of calcite, but did not affect the coexisting dolomite to the same extent. It is noteworthy that the dolomitic fraction of these samples has a mean $\delta^{18}O$ of 9.4 ± 0.4‰. This value is slightly higher than that of dolostones close to the ore (8.6 ± 0.8‰). The difference may be attributed to lower temperature of fluid-rock interaction for incompletely dolomitized rocks, or, alternatively, it may be attributed to the fact that fluid-rock ratios are lower in partially dolomitized rocks and complete equilibration of rocks with the infiltrating fluids was not attained.

In calcitic marbles of La Porteille, the $^{87}Sr/^{86}Sr$ ratio varies between 0.70874 and 0.70937 (Table 1, Fig. 5c). These values are close to those reported for Ordovician carbonates (*Veizer* et al., 1999). Hydrothermal calcites and dolostones have much higher $^{87}Sr/^{86}Sr$ ratios between 0.71081 and 0.71320. Hydrothermal calcites from Pyrenean deposits have variable $^{87}Sr/^{86}Sr$, with the lowest value recorded at the Las Embollas (carbonate-type) deposit.

Hydrothermal minerals

The oxygen and hydrogen isotope compositions of minerals from different talc-chlorite ore deposits are reported in Table 1. The observed $\delta^{18}O$ values with $\delta^{18}O(Qz) > \delta^{18}O(Cal) > \delta^{18}O(Tlc) > \delta^{18}O(Chl)$ are compatible with equilibrium oxygen isotope fractionation among the coexisting hydrothermal minerals (*Zheng*, 1993a and b). In detail, however, the Qz–Cal (Fig. 6a) and Tlc–Chl (Fig. 6d) fractionations give a large range of apparent equilibrium temperatures (200 °C–600 °C) for most deposits. This may be due to incomplete equilibration during hydrothermal mineralization, equilibration at different stages under decreasing temperature conditions or even uncertainties of the geothermometers. The Ceret deposit has lower Qz and Chl oxygen isotope values than other deposits (Fig. 6b). This is probably the result of a lower $\delta^{18}O$ value of the infiltrating fluid rather than that of a higher temperature of interaction, as the Qz–Chl pair gives similar apparent temperature to other deposits (Fig. 6b). In most deposits the oxygen isotope compositions of the minerals are comparable. This allows calculation of a mean $\delta^{18}O$

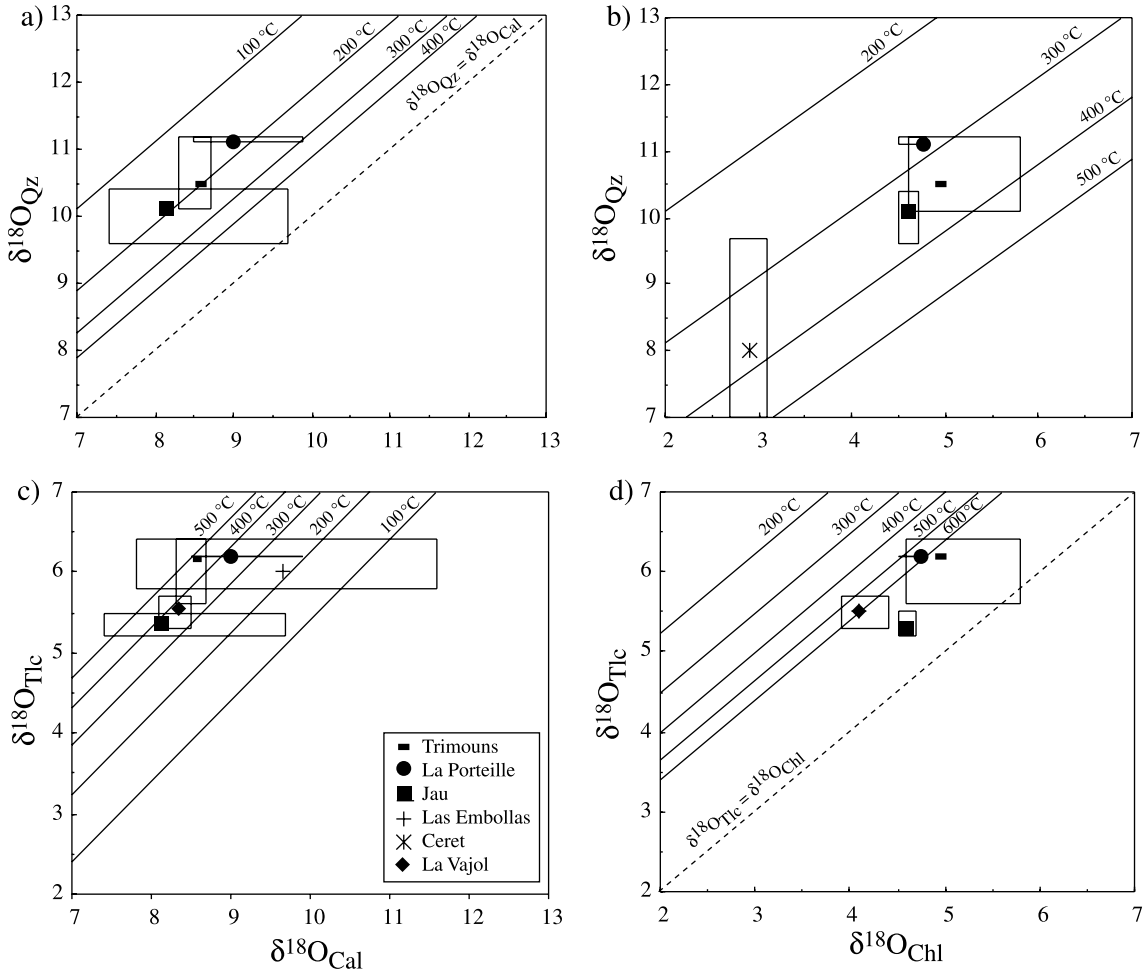

Fig. 6. $\delta^{18}O$ – $\delta^{18}O$ diagram for hydrothermal minerals from Pyrenean talc-chlorite deposits. Symbols refer to mean $\delta^{18}O$ values which are calculated from Table 1. The whole range of $\delta^{18}O$ values variation is reported as a box around mean values. Equilibrium temperature lines are calculated using the fractionation factors of *Zheng* (1993a and b)

value for each mineral: $\delta^{18}O(Cal)_{mean} = 8.7 \pm 1.0‰$, $\delta^{18}O(Qz)_{mean} = 10.5 \pm 0.6‰$, $\delta^{18}O(Tlc)_{mean} = 5.9 \pm 0.4‰$, $\delta^{18}O(Chl)_{mean} = 4.7 \pm 0.4‰$. The Ceret samples have been excluded from this calculation. Provided minerals did not experience significant retrograde isotopic exchange, the intensity of which being governed by different parameters, including oxygen diffusivity in crystals, cooling rate, crystal size and deformation, one can calculate the oxygen isotope composition of water in equilibrium with talc-chlorite deposits at about $\delta^{18}OH_2O = 2$–$4.5‰$ at 300 °C using the fractionation factors of *Zheng* (1993 a and b). In the same conditions, water in equilibrium with the Ceret deposit would have a lower $\delta^{18}O$ value in the range 1–2.8‰.

δD values for talc and chlorite minerals range between −40 and −50‰ with no systematic difference between the two mineral phases. Again, the Ceret deposit is different from other deposits, having a lower δD value (−60‰). The equilibrium hydrogen isotope fractionation factor between talc and water is not known at any

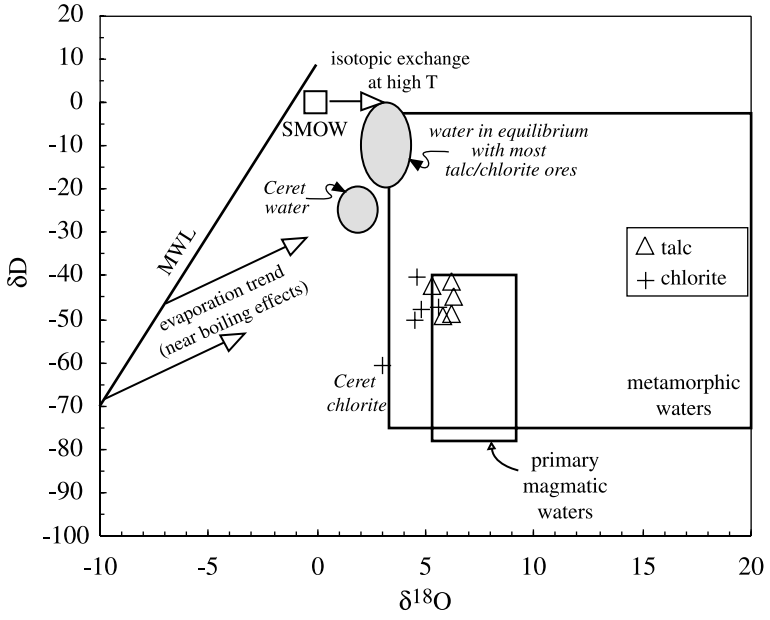

Fig. 7. δD vs. δ^{18}O diagram for talc and chlorite of the Pyrenean deposits. Metamorphic and magmatic water fields are from *Sheppard* (1986). MWL: Meteoric Water Line. Also reported are the field of waters in equilibrium with talc and chlorite from most Pyrenean and Ceret deposit. Arrows describe isotopic effects of different processes

precision. Assuming an hydrogen fractionation factor between chlorite and water of about -30 to -40‰ at 300 °C (*Taylor*, 1974; *Marumo* et al., 1980; *Graham* et al., 1987), one can estimate the hydrogen isotope composition of water in equilibrium with talc-chlorite deposits (except Ceret) to be in the range 0 to -20‰. The δD value of Ceret waters is about -20 to -30‰. The oxygen and hydrogen isotope compositions of these waters are reported in Fig. 7. All water compositions plot close to the limits of the metamorphic fluids field, in the low δ^{18}O – high δD corner, whereas Ceret water is clearly outside this field.

Discussion

Fluid flow and talc-chlorite mineralization

From the location of the compositions in the δD vs. δ^{18}O diagram (Fig. 7), it is unlikely that the mineralising fluids were derived from magmatic rocks. This is consistent with the isotopic signatures of the St. Barthelemy and Pyrenean deposits, which are clearly distinct from those found in deposits formed by contact metamorphism (for example $\delta^{18}O_{Tlc} = 14.8$‰ in the Hwanggangri contact aureole in South Korea; *Shin* and *Lee*, 2002).

The source of the mineralising fluids was probably not related to metamorphic dehydration, as fluid compositions plot at the limit of this potential reservoir (Fig. 7). Furthermore the perturbation of the temperature field associated with the Cretaceous transtension episode was probably not sufficient to dehydrate rocks that had already undergone a metamorphic cycle during Hercynian times. Moreover,

dehydration of the Albian calcareous shales cannot be considered as a potential fluid source because metamorphism of these rocks occurred during the Cenomanian-Turonian period (*Albarède* and *Michard-Vitrac*, 1978; *Golberg* and *Maluski*, 1988), a few million years after talc-chlorite mineralization.

The hydrogen and oxygen isotope compositions of the fluids in equilibrium with the talc-chlorite ore deposits rather suggest an influx of fluids from the surface, mainly from a marine reservoir (Fig. 7). The slightly higher $\delta^{18}O$ value of the mineralising fluids relative to mean sea water isotopic composition might be related to the interaction of water with crustal rocks as indicated by the horizontal arrow in Fig. 7. A similar trend was documented for mid-ocean ridge vents systems (*Bowers* and *Taylor*, 1985). A contribution of modified continental fresh water is also likely, especially for the Ceret deposit. However, the precise composition for these waters is difficult to estimate, as it varies with both altitude and latitude. It is also well documented (*Criss*, 1999) that, while circulating in the crust, water is likely to heat up and reach the boiling point which, in turn, leads to an enrichment in both ^{2}H and ^{18}O (inclined arrows in Fig. 7).

In the Salton Sea Geothermal System, which may be regarded as a modern analog to the Pyrenean system in the Albian (*Choukroune* and *Mattauer*, 1978), some geothermal fluids (*Williams* and *McKibben*, 1989) exhibit many similarities with the talc-forming fluids of the Pyrenees. In particular, some fluids of the Salton Sea System are hypersaline (up to 26 wt% TDS), have reached temperatures of about 300 °C and have $\delta^{18}O$ values in the range 0.5–3‰. However, the δD values of the Pyrenean deposits are clearly different from those of the Salton Sea Geothermal System, the latter have δD values of about −70‰ (*Williams* and *McKibben*, 1989). The hydrogen and oxygen isotope compositions of hydrothermal waters from the Salton Sea System were interpreted as the combined result of evaporation of local continental waters and high-temperature water–rock interactions (*Williams* and *McKibben*, 1989; and references therein). In the Pyrenees, the contribution of Albian seawater is likely to explain the higher δD values of the mineralising fluids. For example, Red Sea hot brines are even characterised by positive δD values (*Pierret* et al., 2001). Figure 8 is a cartoon model of fluid flow in the St. Barthelemy area at the time of mineralization. We propose that the steeply dipping faults limiting the marine pull-apart basins (*Choukroune* and *Mattauer*, 1978) acted as pathways for the downward circulation of marine waters. Crustal-scale fluid circulation was driven by the heat associated with the upward advection of mantle material during extension (*Buck* et al., 1988). This is also corroborated by the good agreement between our Pyrenean data and that of talc that directly precipitated from an active hydrothermal vent in the Gulf of California (*Lonsdale* et al., 1980), which has stable isotope compositions of $\delta^{18}O = 5.3‰$ and $\delta D = -38‰$ at formation temperatures of 280 °C.

During large scale flow, marine waters may have interacted with evaporites, increasing their salinity, as recorded by fluid inclusions (*de Parseval* et al., 1993; *Boiron* et al., 2005). Triassic evaporites are common in the area (*Jarousse* et al., 1981) and a direct contribution of expelled brines from these evaporites buried during extension (Fig. 8) cannot be excluded. Moreover, it is also possible that the mineralizing fluids have interacted with silicate rocks during their migration. This could have led to albitization, which is a widespread process known in the Pyrenees

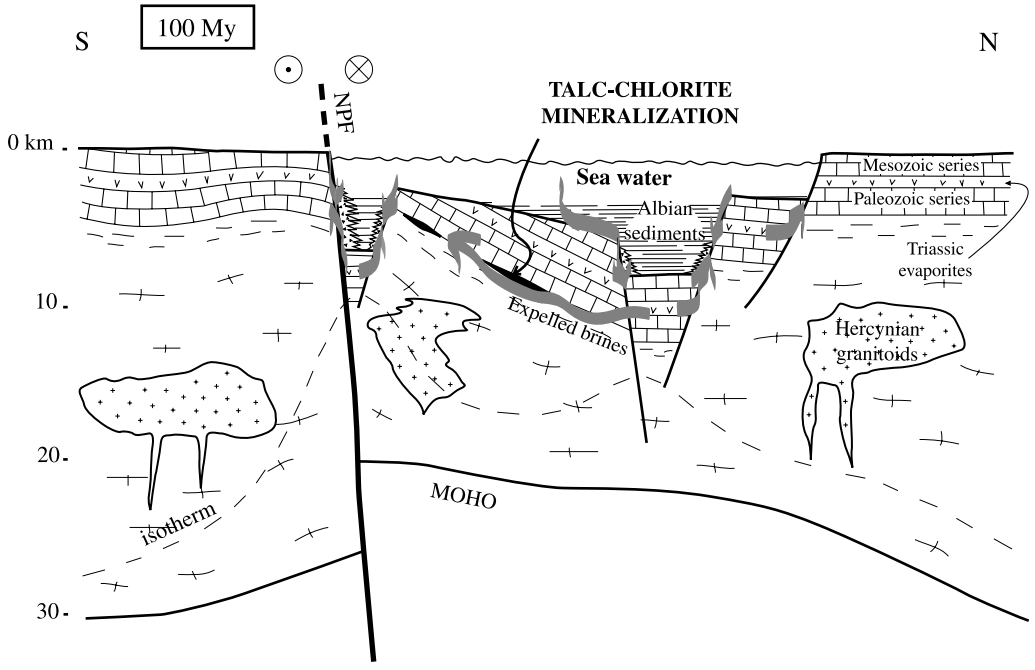

Fig. 8. Schematic cross-section of the north Pyrenean region at 100 Ma (after *Puigdefàbregas* and *Souquet*, 1986; *Roure* et al., 1989) showing a model of fluid circulation during the Albian transtensional context

(*Pascal*, 1979; *Clavières*, 1990), part of albitized rocks formed during the Albian (*Ruffet*, unpublished data). This might have given rise to a decrease of the Na/Ca ratio in the fluids, to reach the low values measured in fluid inclusions (*Boiron* et al., 2005). The low Na/Ca ratio of Salton Sea hypersaline fluids has also been attributed to similar fluid-rock interaction process (*Williams* and *McKibben*, 1989).

From calcitic marbles to dolostones and hydrothermal calcite

The oxygen isotope composition of most calcitic marbles at La Porteille is much lower than that of typical marine carbonate sediments (Fig. 5a). Thus, the calcitic marbles have necessarily undergone some isotopic exchange with externally derived low-$\delta^{18}O$ fluids. Since the isotopic trend defined by calcitic marbles can be extended to the compositions of dolostones and hydrothermal calcites, the entire set of isotopic compositions may be explained as the result of a single fluid-rock interaction event under variable fluid-rock ratios. Figure 5a depicts the isotopic effects of such an infiltration at 300 °C, with a fluid that is characterized by an X_{CO_2} of 0.05. To obtain these estimates, isotopic signatures of the infiltrating fluid were set at $\delta^{18}O_{H_2O} = +3‰$ (see above) and $\delta^{13}C_{CO_2} = -5‰$. Although different $\delta^{13}C$ signatures would be consistent with the measured compositions, the best fit is obtained for this value, intermediate between that, dominant, of marine carbonate and that of organic matter. The carbon isotope composition of organic matter is about $\delta^{13}C = -25‰$ (*de Parseval*, 1992) and organic material is present in the micaschists found in the vicinity of the ore bodies. The isotopic compositions of

all carbonates are thus consistent with a model involving interactions with a single fluid at *ca*. 300 °C, an increasing fluid-rock ratio from the calcitic marbles to the dolostones and ultimately the hydrothermal calcites, and $X_{CO_2} = 0.05$. In a comprehensive mineralogical and geochemical study of talc mineralization in the Bohemian Massif (Fichtelgebirge, Germany), *Hecht* et al. (1999) argued too that the oxygen and carbon isotope evolution recorded by marbles, dolostone and hydrothermal calcite is related to similar increasing fluid-rock ratios.

Most of the geochemical variations recorded in the La Porteille calcitic marbles can also be attributed to metasomatic alteration rather than to sedimentary heritage or diagenetic processes. Firstly, given the small amount of silicate material in the calcitic marbles of La Porteille ($SiO_2 < 1.3\%$, Table 2), high temperature isotope equilibration between a high-$\delta^{18}O$ carbonate phase and a detrital silicate phase with normal $\delta^{18}O$ values ($15 \pm 5‰$; e.g., *Savin* and *Epstein*, 1970a and 1970b) cannot explain the low $\delta^{18}O$ values of the calcitic marbles down to 12.3‰ (Fig. 5a, Table 1). Moreover, the lowest $\delta^{18}O$ value from sample POR 02-10 is found in the vicinity of a dolomitization front and is therefore consistent with isotopic exchange between calcitic marbles and the externally derived fluids. The slightly more radiogenic Sr isotope composition of this sample ($^{87}Sr/^{86}Sr = 0.70934$) is also consistent with the addition of radiogenic Sr from the infiltrating fluids. Secondly, two of the most isotopically altered samples (POR 02-2 and POR 02-4) show Mg enrichment (MgO is about 0.6–0.8 wt%; Table 2) that is unlikely to be sedimentary in origin because growth of fine-grained chlorite porphyroblasts is observed in these two samples in particular. Furthermore, despite of the fact that many calcitic marbles preserved REE + Y patterns typical of sedimentary marine carbonates, the most ^{18}O- and ^{13}C-depleted samples (black circles in Fig. 4a) show LREE depleted patterns. We interpret these patterns as the result of LREE leaching during the metasomatic evolution of the marbles.

Dolostones formed at the expense of calcitic marbles by input of Mg in solution. The Sr concentration in the dolostones ranges between 10 and 57 ppm (*de Parseval*, 1992). This is lower than the Sr concentration of unaltered calcite marbles (200 to 300 ppm), in agreement with the lower mineral-fluid Sr partition coefficient of dolomite compared to calcite. The dolostones are also REE-enriched by one order of magnitude compared to the calcite marbles. They have a $(LREE)_N$ depleted pattern, and do not have a Ce negative anomaly. One sample even displays a positive Eu anomaly.

The Ca and CO_2 liberated during talc formation at the expense of dolostones are likely to combine to form the hydrothermal calcite veins. REE patterns of hydrothermal calcites differ from those of dolostones by larger REE enrichment and a negative Eu anomaly in one case (Fig. 4b), but resemble them in their light REE depletion and an upward slightly convex shape of the REE pattern. This pattern is common in hydrothermal calcites from other places (*Hecht* et al., 1999, and references therein). In natural systems, the shale-normalized REE pattern of hydrothermal fluids that equilibrated with the crustal basement is rather flat (*Michard* and *Albarède*, 1986). This suggests that the fluids from which the calcites of the St. Barthelemy precipitated have been in equilibrium with local crustal metapelites (with a PAAS-like pattern; *de Parseval*, 1992). *Bau* (1991) report the patterns of calcites from Alpine veins that are LREE-depleted relative to the

Pennine gneisses (Zillertal, Austria), which are the local source rocks for REE. However, during calcite precipitation, LREE are preferentially incorporated in the crystal lattice relative to HREE (*Rimstidt* et al., 1998), because of the smaller difference in ionic radius between $LREE^{3+}$ and Ca^{2+} than between $HREE^{3+}$ and Ca^{2+}. The LREE-depleted pattern of the hydrothermal calcites from the St. Barthelemy Massif is thus likely a signature of the fluid itself. The high HREE content of the calcite may be due to the fact that, with increasing alkalinity, hydrothermal fluids dissolve more HREE than LREE (*Michard* and *Albarède*, 1981). As $(LREE)Cl^{2+}$ complexes are more stable in the fluid phase than $(HREE)Cl^{2+}$ complexes (*Steinmann* and *Stille*, 1998) and as Cl^- is the dominant anion in the mineralizing fluid in the area, hydrothermal calcite in equilibrium with such a fluid is likely to display an inverse mirror image of the fluid, namely a LREE-depleted pattern as observed.

Both hydrothermal calcites and dolostones have much more radiogenic Sr compositions than calcite marbles (Table 1), with the high $^{87}Sr/^{86}Sr$ calcites showing the lowest $\delta^{13}C$ (Fig. 5c). This low $\delta^{13}C$ carbon was probably derived from organic matter-rich micaschist levels of the host rocks, suggesting that the most likely Sr source was radiogenic Sr leached from silicate rocks during their transformation into chlorite. It is highly probable that REE, which are enriched in dolostones and hydrothermal calcite, came from this same source. On the other hand, samples from the carbonate-dominated Las Embollas deposit have Sr isotope composition close to those of the protolith (Fig. 5c), which argues for a Sr budget dominated by the host carbonates.

Isotopic record of deformation

Talc-chlorite ores are highly foliated because of shearing. Qualitatively, pressure-solution can be invoked in the studied sample (TRI 00-115, Fig. 3c), where dolomite dissolves at nodule edges exposed to $\sigma 1$ stress. In the mean time, talc crystallised at the expense of dolomite in the pressure shadows because of silica input. External fluids might have been focused in the pressure shadows zones, parallel to $\sigma 3$ stress. Also, the process has followed a reaction like

$$3CaMg(CO_3)_2 + 4SiO_{2(aq)} + H_2O = Mg_3Si_4O_{10}(OH)_2 + 3CaCO_{3(aq)} + 3CO_2$$

which accounts for the pressure shadow samples having lower $\delta^{18}O$ and $\delta^{13}C$ values than those of the nodule (Fig. 5b). The Rayleigh curve of Fig. 5b is a simple approximation of the isotopic effects of such a decarbonation (*Valley*, 1986). It shows that the isotopic evolution of dolomite in the pressure shadows can be explained by decarbonation without involvement of externally derived fluids. A silica-bearing fluid is implied by the growth of talc, but this fluid must have been in isotopic equilibrium with the dolostone at the time of this deformation. As the temperature estimated for decarbonation (300 °C) is close to that prevailing at the time of talc-chlorite mineralization, the shearing event probably occurred during the hydrothermal alteration or in its waning stages under cooling conditions. The shear zones probably acted as conduits for the mineralising fluids, as did the lithological discontinuity defined by the limit between carbonates and silicate rocks.

Conclusion

The main conclusions of this study can be summarized as follows.

The talc-chlorite mineralizations in the Pyrenees record the signature of a mid-crustal fluid circulation, during an Albian transtension event.

The oxygen and hydrogen isotope compositions of talc and chlorite are consistent with a marine origin of the fluids, somewhat modified by isotopic and chemical exchange with crustal rocks. A minor contribution of continental water is suggested for the Ceret deposit, in the eastern part of the area.

The oxygen and hydrogen isotope compositions of dolostones in the St. Barthelemy Massif show that they formed by interaction between the mineralising fluids and the calcitic marbles, the composition of which was also modified by interaction with these fluids at low fluid-rock ratios. Hydrothermal calcites recorded the highest fluid-rock ratios.

Carbonates-fluid interaction led to REE enrichment and fractionation, and an influx of radiogenic Sr. These elements probably come from silicate rocks transformed into chlorite.

Acknowledgements

The authors wish to thank *Bernard Moine* for introducing *PB* to the problematic related to talc mineralization. *Michel de Saint-Blanquat* helped during field work. Part of this work was undertaken during an MSc project (*AD'h*). *Jean Cornichet* provided much help during analytical sessions. *Nicole Morin* made the Sr isotope analyses. *Pierre Agrinier* (IPGP) is thanked for making the hydrogen analyses possible. A preliminary version of the manuscript was improved through the review of *Serge Fourcade*. Reviews of *Elizabeth King* and an anonymous reviewer helped to clarify some ideas. *Jean Braun* improved the English. The editorial help of *Paolo Garofalo* and *Rainer Abart* was greatly appreciated.

References

Abzalov MZ (1998) Chrome-spinels in gabbro-wehrlite intrusions of the Pechenga area, Kola Peninsula, Russia: emphasis on alteration features. Lithos 43: 109–134

Al-Aasm I, Taylor BE, South B (1990) Stable isotope analysis of multiple carbonate samples using selective acid extraction. Chem Geol 80: 119–125

Albarède F, Michard-Vitrac A (1978) Age and significance of the North Pyrenean metamorphism. Earth Planet Sci Lett 40: 327–332

Bau M (1991) Rare-earth element mobility during hydrothermal and metamorphic fluid-rock interaction and the significance of the oxydation state of europium. Chem Geol 93: 219–230

Bigeleisen J, Perlman ML, Posser HC (1952) Conversion of hydrogenic materials to hydrogen for isotopic analyses. Anal Chem 24: 1356–1357

Blount AM, Vassiliou AH (1980) The mineralogy and origin of the talc deposits near Winterboro, Alabama. Econ Geol 75: 107–116

Boiron M-C, Boulvais P, Cathelineau M, Calvayrac N, Hubert G, Banks D (2005) Fluid circulation at the origin of the Trimouns talc deposit (Pyrenees, France). ECROFI XVIII meeting, Siena. (Electronic material)

Bottinga Y (1968) Calculation of fractionation factors for carbon and oxygen isotopic exchange in the system calcite-carbon dioxide-water. J Phys Chem 72: 800–808

Bowers TS, Taylor HP (1985) An integrated chemical and stable-isotope model for the origin of midocean ridge hot spring systems. J Geophys Res 90: 12,583–12,606

Brady JB, Cheney JT, Rhodes AL, Vasquez A, Green C, Duvall M, Kogut A, Kaufman L, Kovaric D (1998) Isotope geochemistry of proterozoic talc occurences in Archean marbles of the Ruby Mountains, southwest Montana, USA. Geol Mat Res 1: 1–41

Buck WR, Martinez F, Steckler MS, Cochran JR (1988) Thermal consequences of lithospheric extension: pure and simple. Tectonics 7: 213–234

Carreras J (2001) Zooming on Northern Cap de Creus shear zones. J Struct Geol 23: 1457–1486

Choukroune P (1992) Tectonic evolution of the Pyrenees. Ann Rev Earth Planet Sci 20: 143–158

Choukroune P, Le Pichon X, Seguret M, Sibuet JC (1973) Bay of Biscay and Pyrenees. Earth Planet Sci Lett 18: 109–118

Choukroune P, Mattauer M (1978) Tectonique des plaques et Pyrénées: sur le fonctionnement de la faille transformante nord-pyrénéenne; comparaisons avec les modèles actuels. Bull Soc Géol France 20: 689–700

Clavières V (1990) Muscovitisation et feldspathisation hydrothermale dans le massif granitique de Millas (Pyrénées Orientales). Géométrie, Géochimie, Modélisation. Unpub. PhD thesis, University of Paris VI, 194 pp

Clayton RN, Mayeda TK (1963) The use of bromine pentafluorine in the extraction of oxygen from oxides and silicates for isotopic analysis. Geochim Cosmochim Acta 27: 43–52

Criss RE (1999) Principles of stable isotope distribution. Oxford University Press, 254 pp

de Parseval P (1992) Minéralogie et géochimie du gisement de talc de Trimouns (Pyrénées, France). Unpub. PhD thesis, Toulouse, 227 pp

de Parseval P, Moine B, Fortune JP, Ferret J (1993) Fluid-mineral interactions at the origin of the Trimouns talc and chlorite deposit (Pyrénées, France). In: *Fenoll Hach-Ali P, Torrez-Ruiz J, Gervilla F* (eds) Current research in Geology applide to ore deposits. Granada, pp 205–208

de Saint-Blanquat M, Lardeaux JM, Brunel M (1990) Petrological arguments for high temperature extensional deformation in the Pyrenean variscan crust (Saint-Barthélémy massif, Ariège, France). Tectonophysics 177: 245–262

El-Sharkawy MF (2000) Talc mineralization of ultramafic affinity in the Eastern Desert of Egypt. Mineral Dep 35: 346–363

Fortuné JP (1971) Contribution à l'étude minéralogique et génétique des talcs pyrénéens. Unpub. Thesis, Toulouse, 227 pp

Franceschelli M, Carcangiu G, Caredda AM, Crugiani G, Memmi I, Zucca M (2002) Transformation of cumulate mafic rocks to granulite and re-equilibration in amphibolite and greenschist facies in NE Sardinia, Italy. Lithos 63: 1–18

Gleizes G, Leblanc D, Bouchez JL (1997) Variscan granites of the Pyrenees revisited: their role as syntectonic markers of the orogen. Terra Nova 9: 38–41

Gleizes G, Leblanc D, Bouchez JL (1998) The main phase of the Hercynian orogeny of the Pyrenees is a dextral transpression. In: *Holdsworth RE, Stracham RA, Dewey JF* (eds) Continental transpressional and transtensional tectonics. Geol Soc London Spec Pub 135: 267–273

Golberg JM, Maluski H (1988) Données nouvelles et mise au point sur l'âge du métamorphisme pyrénéen. C R Acad Sci Paris 306: 429–435

Graham CM, Viglino JA, Harmon RS (1987) Experimental study of hydrogen-isotope exchange between aluminous chlorite and water and of diffusion in chlorite. Am Min 72: 566–579

Hecht L, Freiberger R, Gilg HA, Grundmann G, Kostitsyn YA (1999) Rare earth element and isotope (C, O, Sr) characteristics of hydrothermal carbonates: genetic implications for dolomite-hosted talc mineralization at Göpfersgrün (Fichtelgebirge, Germany). Chem Geol 155: 115–130

Jarousse J, Moine B, Sauvan P (1981) Etude pétrographique et géochimique des métasédiments évaporitiques du Trias pyrénéen. Comparaison avec le Trias du Bassin d'Aquitaine. Bull Soc Géol France 23: 377–386

Lonsdale PF, Bischoff JL, Burns VM, Kastner M, Sweeney RE (1980) A high-temperature hydrothermal deposit on the Seabed at a Gulf of California spreading center. Earth Planet Sci Lett 49: 8–20

Marumo K, Nagasawa K, Kuroda Y (1980) Mineralogy and hydrogen isotope composition of clay minerals in the Ohnuma geothermal area, northeastern Japan. Earth Planet Sci Lett 47: 255–262

McCrea JM (1950) On the isotope chemistry of carbonates and a paleotemperature scale. J Chem Phys 18: 849–857

McLennan SM (1989) Rare earth elements in sedimentary rocks: influence of provenance and sedimentary processes. In: *Lipin BR, McKay GA* (eds) Geochemistry and mineralogy of Rare Earth Elements. Rev Min Geochem 21: 169–200

Michard A, Albarède F (1986) The REE content of some hydrothermal fluids. Chem Geol 55: 51–60

Moine B, Fortuné JP, Moreau P, Viguier F (1989) Comparative mineralogy, geochemistry and conditions of formation of two metasomatic talc and chlorite deposits: Trimouns (Pyrénées, France) and Rabenwald (Eastern Alps, Austria). Econ Geol 84: 1398–1416

Nothdurft LD, Webb GE, Kamber BS (2004) Rare earth element geochemistry of late Devonian reefal carbonates, Canning Basin, Western Australia: Confirmation of a seawater REE proxy in ancient limestones. Geochim Cosmochim Acta 68: 263–283

Ohmoto H, Rye RO (1979) Isotopes of sulfur and carbon. In: *Barnes HL* (ed) Geochemistry of hydrothermal ore deposits, pp 509–561

Olivet JL (1996) La cinématique de la plaque ibérique. Bull Cent Rech Explor-Prod Elf Aquitaine 20: 131–195

O'Neil JR, Epstein S (1966) A method for oxygen isotope analysis of milligram quantities of water and some of its applications. J Geophys Res 71: 4955–4961

Pascal M-L (1979) Les albitites du massif de l'Agly (Pyrénées Orientales). Unpub. PhD thesis, Ecole Nationale Supérieure des Mines, Paris, France, 163 pp

Pierret MC, Clauer N, Bosch D, Blanc G, France-Lanord C (2001) Chemical and isotopic ($^{87}Sr/^{86}Sr$, $\delta^{18}O$, δD) constraints to the formation processes of Red-Sea brines. Geochim cosmochim Acta 65: 1259–1275

Puigdefàbregas C, Souquet P (1986) Tecto-sedimentary cycles and depositional sequences of the Mesozoic and Tertiary from the Pyrenees. Tectonophysics 129: 173–203

Rimstidt JD, Balog A, Webb J (1998) Distribution of trace elements between carbonate minerals and aqueous solutions. Geochim Cosmochim Acta 62: 1851–1883

Roure F, Choukroune P, Berastegui X, Munoz JA, Villien A, Matheron P, Bareyt M, Seguret M, Camara P, Deramond J (1989) ECORS deep seismic data and balanced cross sections: geometric constraints on the evolution of the Pyrenees. Tectonics 8: 41–50

Savin SM, Epstein S (1970a) The oxygen and hydrogen isotope geochemistry of clay minerals. Geochim Cosmochim Acta 34: 25–42

Savin SM, Epstein S (1970b) The oxygen and hydrogen isotope geochemistry of ocean sediments and shales. Geochim Cosmochim Acta 34: 323–329

Schandl ES, Sharara NA, Gorton MP (1999) The origin of the Atshan talc deposit in the Hamata area, Eastern Desert, Egypt: a geochemical and mineralogical study. Can Min 37: 1211–1227

Schärer U, de Parseval P, Polvé M, de Saint Blanquat M (1999) Formation of the Trimouns talc-chlorite deposit (Pyrenees) from persistent hydrothermal activity between 112 and 97 Ma. Terra Nova 11: 30–37

Sheppard SMF (1986) Stable isotope variations in natural waters. In: *Valley JW, Taylor HP, O'Neil JR* (eds) Stable isotopes in high temperature geologic processes. Rev Min Geochem 16: 319–372

Sheppard SMF, Schwarcz HP (1970) Fractionation of carbon and oxygen isotopes and magnesium between coexisting calcite and dolomite. Contrib Mineral Petrol 26: 161–198

Shin D, Lee I (2002) Carbonate-hosted talc deposits in the contact aureole of an igneous intrusion (Hwanggangri mineralized zone, South Korea): geochemistry, phase relationships, and stable isotope studies. Ore Geol Rev 22: 17–39

Soula JC, Debat P, Deramond J, Pouget P (1986) A dynamic model of the structural evolution of the Hercynian Pyrenees. Tectonophysics 129: 29–51

Steinmann M, Stille P (1998) Strongly fractionated REE patterns in salts and their implications for REE migration in chloride-rich brines at elevated temperatures and pressures. C R Acad Sci Paris 327: 173–180

Taylor HP (1974) The application of oxygen and hydrogen isotope studies to problems of hydrothermal alteration and ore deposition. Econ Geol 69: 843–883

Taylor HP (1977) Water/rock interaction and the origin of H_2O in granitic batholiths. J geol Soc Lond 133: 509–558

Tesalina SG, Nimis P, Augé T, Zaykov VV (2003) Origin of chromite in mafic/ultramafic-hosted hydrothermal massive sulfides from the Main Uralian Fault, South Urals, Russia. Lithos 70: 39–59

Tornos F, Spiro BF (2000) The geology and isotope geochemistry of the talc deposits of Puebla de Lillo (Cantabrian zone, Northern Spain). Econ Geol 95: 1277–1296

Valley JW (1986) Stable isotope geochemistry of metamorphic rocks. In: *Valley JW, Taylor HP, O'Neil JR* (eds) Stable isotopes in high temperature geologic processes. Rev Min Geochem 16: 445–489

Veizer J, Ala D, Azmy K, Bruckschen P, Buhl D, Bruhn F, Carden GAF, Diener A, Ebneth S, Godderis Y, Jasper T, Korte C, Pawallek F, Podlaha OG, Strauss H (1999) $^{87}Sr/^{86}Sr$, $\delta^{13}C$ and $\delta^{18}O$ evolution of Phanerozoic seawater. Chem Geol 161: 59–88

Williams AE, McKibben MA (1989) A brine interface in the Salton Sea Geothermal System, California: Fluid geochemical and isotopic characteristics. Geochim Cosmochim Acta 53: 1905–1920

Zheng YF (1993a) Calculation of oxygen isotope fractionation in anhydrous silicate minerals. Geochim Cosmochim Acta 57: 1079–1091

Zheng YF (1993b) Calculation of oxygen isotope fractionation in hydroxyl-bearing silicates. Earth Planet Sci Lett 120: 247–263

Zheng YF (1999) Oxygen isotope fractionation in carbonate and sulfate minerals. Geochem J 33: 109–129

Authors' addresses: P. Boulvais (corresponding author; e-mail: philippe.boulvais@univ-rennes1.fr), Géosciences Rennes – UMR 6118, Université de Rennes I, Campus de Beaulieu, 35042 Rennes cedex, France; P. de Parseval (e-mail: parseval@lmtg.obs-mip.fr), Observatoire Midi-Pyrénées – LMTG – UMR5563, 14 avenue Edouard Belin, 31400 Toulouse, France; A. D'Hulst (e-mail: alan.dhulst.1@ulaval.ca), Département de géologie et de génie géologique, Faculté des sciences et de génie, Université Laval, Sainte-Foy, Québec, Canada G1K 7P4; P. Paris (e-mail: pierre.paris@europe.luzenac.com), Talc de Luzenac France, BP 11, 09250 Luzenac cedex, France